

Phase Locking, Devil's Staircases, Farey Trees, and Arnold Tongues in Driven Vortex Lattices with Periodic Pinning

C. Reichhardt and Franco Nori

Department of Physics, The University of Michigan, Ann Arbor, Michigan 48109-1120

(August 1, 2018)

Abstract

Using numerical simulations, we observe phase locking, Arnold tongues, and Devil's staircases for vortex lattices driven at varying angles with respect to an underlying superconducting periodic pinning array. This rich structure should be observable in transport measurements. The transverse $V(I)$ curves have a Devil's staircase structure, with plateaus occurring near the driving angles along symmetry directions of the pinning array. Each of the plateaus corresponds to a different dynamical phase with a distinctive vortex structure and flow pattern.

PACS numbers: 74.60.Ge, 64.70.Rh, 74.60.Jg

Introduction.— Numerous nonlinear driven systems in physics, astronomy, and engineering exhibit striking responses with complex phase-locking plateaus characterized by Devil’s staircases, Arnold tongues, and Farey trees [1–4]. Here, we present the first evidence that these structures can be observed in bulk superconductors.

Driven vortex lattices (VLs) interacting with either random or periodic disorder have attracted growing interest due to the rich variety of nonequilibrium dynamic phases which are observed in these systems. These phases include the elastic and plastic flow of vortices which can be related to VL order and transport properties [5–9]. Periodic pinning arrays interacting with VLs are now attracting increasing attention as recent experiments with patterns of holes [10] and magnetic dots [11] have produced interesting commensurability effects and enhanced pinning. These systems are an excellent realization of an elastic lattice interacting with a periodic substrate that is found in a wide variety of condensed matter systems including charge-density-waves, Josephson-junction arrays, and Frenkel-Kontorova-type models of friction (see, e.g., [12]). An interesting aspect of periodic pinning arrays that has not been addressed so far is how the symmetry properties of the array affect the transport properties as the VL is driven at different angles.

We find that as a slowly increasing transverse force is applied to a VL already moving in the longitudinal direction, the VL undergoes a remarkable series of *locking transitions* that significantly affect both the VL ordering and transport properties. These locking phases occur when the direction of the vortex motion locks with a symmetry direction of the pinning array. As the VL passes through these phases, the transverse velocity component as a function of increasing transverse drive shows a series of plateaus which form a Devil’s staircase structure [1–3]. At the boundaries of certain locked phases the VL undergoes a transition to a *plastic flow* phase in which defects are generated in the VL. In the locked phases the VL undergoes *elastic* flow in static 1D channels and the overall VL has a variety of orderings, including triangular and square.

Simulation.— We consider a 2D slice of N_v 3D rigid vortices interacting with a square array of N_p parabolic wells, with lattice constant a , and periodic boundary conditions. We

integrate [8] the equations of vortex motion $\mathbf{f}_i = \mathbf{f}_i^{vv} + \mathbf{f}_i^{vp} + \mathbf{f}_d = \eta \mathbf{v}_i$. The total force \mathbf{f}_i on vortex i includes interactions with other vortices \mathbf{f}_i^{vv} , pinning \mathbf{f}_i^{vp} by parabolic wells, and an applied driving force $\mathbf{f}_d = f_x \hat{\mathbf{x}}$. The vortex-vortex interaction between vortex i and the other N_v vortices is $\mathbf{f}_i^{vv} = \sum_{j=1}^{N_v} f_0 K_1(|\mathbf{r}_i - \mathbf{r}_j|/\lambda) \hat{\mathbf{r}}_{ij}$, where $K_1(r/\lambda)$ is a modified Bessel function, λ is the penetration depth, $f_0 = \Phi_0^2/8\pi^2\lambda^3$, $\hat{\mathbf{r}}_{ij} = (\mathbf{r}_i - \mathbf{r}_j)/|\mathbf{r}_i - \mathbf{r}_j|$, and we set $\eta = 1$. All lengths, fields, and forces are given in units of λ , Φ_0/λ^2 , and f_0 , respectively. For most of the results presented here the number of vortices is close to the number of pinning sites, $N_v = 1.062N_p$. We have conducted a series of simulations with different pinning parameters so that accurate phase diagrams of the dynamic phases can be obtained. In order to investigate finite size effects we have examined system sizes varying between $36\lambda \times 36\lambda$ and $108\lambda \times 108\lambda$, with N_v between $N_v = 550$ and $N_v = 4955$.

Voltage-Current Response.— First, the VL ground state at zero applied driving force is found by simulated annealing (i.e., by cooling the VL from high- T). After a low energy ground state is found, a slowly increasing driving force, f_x , is applied along the horizontal symmetry axis of the square pinning. We find that increasing f_x in increments of $0.001f_0$ every 400 MD steps, from $f_x = 0$ to $f_x = 3.0f_0$, is slow enough that the vortex dynamics does not depend on the rate of increase of f_x . Once f_x is brought to $3.0f_0$ it is held constant while a force, which we label f_y , is applied in the transverse or y -direction. We increase f_y from 0 to $3.25f_0$, also in increments of $0.001f_0$ every 400 MD steps. The total driving force has a net magnitude of $f_d = (f_x^2 + f_y^2)^{1/2}$ at an angle $\theta = \tan^{-1}(f_y/f_x)$ with respect to the x -direction. We compute the average velocity of the moving vortices in both the longitudinal $V_x = (1/N_v) \sum_{i=1}^{N_v} \mathbf{v}_i \cdot \hat{\mathbf{x}}$ and the transverse $V_y = (1/N_v) \sum_{i=1}^{N_v} \mathbf{v}_i \cdot \hat{\mathbf{y}}$ direction, as f_y is increased. Velocity versus driving plots correspond to experimentally measurable voltage-current $V(I)$ curves.

In Fig. 1(a) we present a typical plot of V_x and V_y . For $f_y \lesssim 0.4f_0$, $V_y = 0$ indicating that the VL is *pinned* in the y -direction even though the VL is moving in the x -direction. Depinning in the transverse direction occurs at $f_y = 0.4f_0$, as indicated by the sharp jump up in V_y . We label this critical transverse depinning force f_y^c . A jump up in V_x is also observed

at f_y^c . As f_y is linearly increased, V_y does *not* grow linearly but instead in a remarkable series of *jumps* and *plateaus* of varying sizes [3]. Along the plateaus V_y is constant or increasing very slowly, indicating that the vortex motion is *locked* in a certain direction for a finite range of increasing f_y . The small jumps and dips in V_x correspond to the onset of plateaus in V_y . The plateaus in V_y occur when the ratio of f_y to f_x is near a rational value: $f_y/f_x = p/q$, where p and q are integers. In Fig. 1(a) the largest plateaus occur at $p/q = 0, 1/3, 1/2, 2/3$ and 1. Fig. 1(b) shows a blow-up of a region in Fig. 1(a) for values of $f_y = 0.6f_0$ to $2.1f_0$, where additional plateaus at $p/q = 1/5, 1/4, 2/5, 3/7$, and $3/5$ are highlighted. For larger system sizes we find exactly the same behavior in V_y and V_x as observed in Fig. 1, indicating that it is independent of the system size.

Vortex Dynamics and the Origin of the Plateaus.— To understand why the plateaus occur as well as the VL dynamics in the plateau and non-plateau regions, in Fig. 2(a-d) we plot the vortex trajectories for rational ratios of $f_y/f_x = 0, 1/2, 1$, and the irrational ratio $f_y/f_x = 2\pi/11 = 0.571\dots$. In Fig. 2(a), where $f_y < f_y^c$, the vortex motion traverses pin sites periodically and it is only along the x -direction—with the vortex flow restricted in 1D paths *along* the pinning rows. This periodic 1D motion persists up to $f_y = f_y^c$, at which point the vortices also begin to flow in the y -direction. In Fig. 2(b), for $p/q = 1/2$ where a large plateau in V_y is observed in Fig. 1, the vortices again exhibit periodic motion and flow in 1D channels *along* the pinning sites—and along a symmetry axis of the pinning array at an angle $\theta = \tan^{-1}(1/2)$ from the x -axis. A similar periodic 1D motion is seen in (d) for $f_y/f_x = 1$, with the VL motion at 45° from the x -axis. In Fig. 2(c), at the irrational f_y/f_x ratio, the vortex trajectories are different than those observed in Fig. 2(a,b,d). Here the quasiperiodic vortex trajectories drift over time, eventually covering the sample (i.e., ergodic-like motion). In general, the plateau regions (with rational f_y/f_x) in $V_y(I)$ correspond to periodic 1D vortex trajectories, while the non-plateau regions produce quasiperiodic trajectories [1,2,13].

To understand how the vortex motion locks into certain driving angles, we first consider the case $f_y/f_x = 0$. Here the vortices move along the pinning rows in 1D paths, with each vortex traversing a distance $a - 2r_p$ between pinning sites, as seen in Fig. 2(a). An

application of a transverse force f_y causes the moving vortices to drift a small distance in the y -direction. Once the vortices interact with the pinning sites, they feel a force that moves them towards the center of the pinning site which keeps them locked along the x -direction. When f_y is large enough, $f_y^c \gtrsim f_x \tan(r_p/a)$ [13], the vortices are able to break off from moving only along the x -direction and start moving in the y -direction as well.

As f_y is increased beyond f_y^c , the net driving force vector will be at an angle with the horizontal. Due to the symmetry of the square pinning array, along the angles where $\theta = \tan^{-1}(p/q)$, the vortices encounter pinning sites *periodically* spaced a distance a_θ apart. This distance is related to the pinning lattice constant a by $a_\theta = a(p^2 + q^2)^{1/2}$. Along these commensurate angles, the vortex motion will be periodic and locked in 1D channels in a similar manner as the $f_y/f_x = 0$ case. The force needed to depin the vortices from the commensurate angles will vary since a_θ varies. For values where a_θ is small, the vortices will move only a small distance between pinning sites, so a higher depinning force is needed. For large a_θ the vortices will move a much longer distance before encountering the pinning sites, so a much smaller depinning force is needed. This is in agreement with Fig. 1 where the *largest* plateaus (due to enhanced pinning) occur for values of p/q that produce the lowest distance between pinning sites, that is the *smallest* a_θ (i.e., $p/q = 0/1, 1/1, \text{ and } 1/2$).

The onset of certain plateaus coincide with a variety of *structural* transitions in the VL. We quantify this angle-dependent evolving *topological order* by using the Voronoi (or Wigner-Seitz) construction to obtain the fraction of vortices with coordination numbers six, P_6 , and four, P_4 . In Fig. 3(a,b) we show the evolution of P_6 and P_4 as f_y is increased, for the same system as in Fig. 1. For $f_y < f_y^c$, $P_6 \approx 0.68$, indicating a mostly triangular VL. At $f_y = f_y^c$, a dip in P_6 , along with direct observation of the VL flow, show that the VL *disorders* due to *plastic* deformations. Right after the initial dip in P_6 the VL suddenly regains considerable triangular ordering, as indicated by $P_6 \approx 0.95$. Small dips in P_6 can be seen near the $1/4, 1/3, \text{ and } 2/3$ locking regions. At the $1/2$ locking region the VL is considerably disordered, as indicated by the sharp drop in P_6 . This is consistent with Fig. 3(c), where both the vortex positions and Voronoi polygons are shown for a $12\lambda \times 12\lambda$

region in the $1/2$ locking region. At the $1/1$ locking region P_6 drops almost to zero while P_4 increases to about 0.9, indicating a structural phase transition from a triangular to a *square* VL. Here, the $f_y = f_x$ symmetric drive is what produces a moving square VL. The less symmetric drives ($2f_y = f_x$ and $3f_y = f_x$), produce more distorted squares [13]. For the special case when $f_y = 0$ and for the B used in Fig. 3, correlations between nearby VL rows are strong, and near $2/3$ of the VL has triangular order (which diminishes for weaker B 's). In Fig. 3(d,e) the vortex positions and Voronoi polygons are shown for (d) right *before* the transition to the $1/1$ locking region and (e) *in* the $1/1$ locking region showing the triangular and square ordering of the VL respectively. Right *at* the boundaries of the $1/1$ phase, the VL is strongly disordered and has a similar structure to Fig. 3(c).

Phase Diagrams with Arnold Tongues.— We have derived *five phase diagrams* which indicate the evolution of the plateau regions versus the following parameters: f_p , n_p , r_p , commensurability, and disorder. These five phase diagrams are all very similar, and thus here we present only one: Fig. 4(a). This is obtained by conducting a series of simulations in which the maximum pinning force f_p is varied between $0.25 \leq f_p/f_0 \leq 2.75$. The phase diagram shows 18 clearly defined (shaded) *Arnold tongues* or plateaus [1–4]. As f_p is decreased the widths of the tongues also show a corresponding decrease. For $f_p/f_0 > 2.5$ several locking phases are lost (i.e., $1/6$, $4/7$, $5/6$) due to overlapping by other locking regions. For $f_p/f_0 < 1.0$ only the strongest plateau regions can be resolved within the accuracy of our calculations.

The phase diagram in Fig. 4(a) has the *same* structure as Arnold tongues [1–4] found in phase locking systems where the widths of the tongues, or locking regions, increase as the nonlinear coupling increases. Here, the coupling is between the vortices and the pinning array, and is increased with increasing f_p , r_p , n_p , density of vortices (i.e., the commensurability B/B_ϕ), and pin-location order [13]. In Fig. 4(b) we present the width of the $0/1$ locking region for varying pinning density in units of the pinning lattice constant a . As a decreases the width of the locked region increases. This can be understood by considering that as a decreases the vortices in the locked region will move a smaller distance between

pinning sites; thus a higher transverse force is needed to break the vortices away from the locked region. The widths of the other locked regions show the same behavior as the 0/1 region for increasing a [13].

We have also examined the effects of pin disorder on the width of the locking regions by conducting a series of simulations in which the pinning sites are randomly displaced up to an amount δr away from the perfectly square pinning lattice. We consider the case where $\delta r = a/2$ to be a good approximation to a random pinning array. In Fig. 4(c), we examine how the width of the 0/1 locking region, f_y^c , decreases as δr is increased. It is of interest to compare our results for large disorder with Ref [6](a) in which a nonzero transverse critical force f_y^c was predicted. Recent $T = 0$ MD simulations have observed extremely small transverse barriers [6](b). We find that for large disorder, $\delta r = a/2$, a true transverse barrier (i.e., $V_y = 0$) is *not* observed. Also, for a triangular array of pins, the plateaus occur for $\theta = \tan^{-1}(\sqrt{3}p/(2q + 1))$.

Summary.— In conclusion, we have found that as an increasing transverse force is applied to a strongly driven VL interacting with a periodic pinning array, the VL undergoes a remarkable series of locking transitions in which both the VL order and flow patterns change. As the VL passes through these transitions, V_y exhibits a striking series of plateaus forming a Devil’s staircase structure. The width variations of these plateaus with different pinning form Arnold tongues which can be indexed via a Farey tree construction. These locking effects occur whenever the VL is driven along a symmetry angle of the pinning array. For a square pinning array, the locking phases occur when driving in the longitudinal direction is a rational ratio, $f_y/f_x = p/q$. These predictions can be tested experimentally and we hope that this work will motivate several novel experiments. Moreover, other candidate systems where these predictions may be accessible include: driven Wigner crystals interacting with a periodic array of donors, driven colloids interacting with optical-trap arrays, spin- and charge-density waves, Josephson-junction arrays, and solid friction experiments.

We thank F. Marchesoni, M. Bretz, and very specially C.J. Olson for useful discussions.

REFERENCES

- [1] H.G. Shuster, *Deterministic Chaos* (VCH Verlag, Weinheim, 1988); E. Ott, *Chaos* (Cambridge, New York, 1993); P. Bak, *Physics Today* **39**, 38 (1986).
- [2] Such structures are found in numerous nonlinear systems in nature [1] and are indicative of phase locking (i.e., when the ratio w , known as the winding number, of two competing frequencies is a rational number p/q). Orbits are periodic when w is rational, and quasiperiodic (space-filling, or ergodic, for large times) otherwise [1]. Note that here there is *no external AC* driving as in previous systems (e.g., charge density waves and Josephson junctions) that exhibited these phase-locking plateaus [1]. Here the two frequencies are internal: from the VL motion along the x and y directions.
- [3] The overall structure of the transverse voltage $V_y(I)$ is that of a Devil's *staircase* [1], in which plateaus appear at rational ratios of $f_y/f_x = p/q$ with the largest plateaus occurring when p/q has the smallest denominator, in agreement with Fig. 1. The hierarchy of plateau sizes follows the *Farey tree* construction [1], which orders all rationals in $[0, 1]$ with increasing denominators q according to the rule that the largest plateau between p/q and p'/q' is $(p+p')/(q+q')$, and orders all mode-locking steps with $w = p/q$ according to their decreasing widths [1].
- [4] Note that Arnold tongues are typically studied in the context of nonlinear circle maps with *two* degrees of freedom [1]. Here we have *very many* degrees of freedom which are interacting with each other, and also with numerous sites in the substrate. Moreover our dynamics is *continuous*, not a *discrete* map. Thus, our VL system is far more complex than the standard discrete 2D maps used to describe phase-locked structures.
- [5] L. Balents *et al.* *Phys. Rev. B* **57**, 7705 (1998); S. Spencer and H.J. Jensen, *ibid.* **55**, 8473 (1997); A.E. Koshelev and V.M. Vinokur, *Phys. Rev. Lett.* **73**, 3580 (1994).
- [6] (a) T. Giamarchi and P. Le Doussal, *Phys. Rev. B* **57**, 11 356 (1998); (b) K. Moon, R.T. Scalettar, and G.T. Zimanyi, *Phys. Rev. Lett.* **77**, 2778 (1996).
- [7] S. Bhattacharya and M.J. Higgins, *Phys. Rev. Lett.* **70**, 2617 (1993); U. Yaron *et al.*

- Nature **376**, 753 (1995).
- [8] C. Reichhardt, C.J. Olson, and F. Nori, Phys. Rev. Lett. **78**, 2648 (1997).
- [9] F. Nori, Science **271**, 1373 (1996); C. Reichhardt *et al.*, Phys. Rev. B **58**, 7937 (1998); **54**, 16108 (1996).
- [10] T. Matsuda *et al.*, Science **271**, 1393 (1996); K. Harada *et al.*, *ibid.* **274**, 1167 (1996); M. Baert *et al.*, Phys. Rev. Lett. **74**, 3269 (1995); J.Y. Lin *et al.*, Phys. Rev. B **54**, R12 714 (1996); A. Castellanos *et al.*, Appl. Phys. Lett. **71**, 962 (1997).
- [11] J.I. Martín *et al.*, Phys. Rev. Lett. **79**, 1929 (1997); D.J. Morgan and J.B. Ketterson, *ibid.* **80**, (1998).
- [12] *Charge Density Waves in Solids*, edited by L.P. Gorkov and G. Gruner (Elsevier, New York, 1989); S.E. Hebboul and J.C. Garland, Phys. Rev. B **47**, 5190 (1993); L.M. Floría and F. Faló, *ibid.* **68**, 2713 (1992); O.M. Braun, *et al.*, *ibid.* **78**, 1295 (1997).
- [13] C. Reichhardt and F. Nori, unpublished. Magnified figures are in www-personal.engin.umich.edu/~nori

FIGURES

FIG. 1. (a) Average longitudinal V_x (upper curve) and transverse V_y velocities versus the transverse driving force f_y for a $36\lambda \times 36\lambda$ sample with a square pinning array, density of field lines B satisfying $B/B_\phi = 1.062$, matching field $B_\phi = 0.4 \Phi_0/\lambda^2$, density of pinning sites $n_p = 0.4/\lambda^2$, $f_p = 2.5f_0$, $a = 1.57\lambda$, and $r_p = 0.3\lambda$. f_x is fixed at $f_x = 3.0f_0$. Plateaus are seen in V_y near values where $f_y/f_x = p/q$, where p and q are integers. The largest plateaus (at $0/1$, $1/3$, $1/2$, $2/3$, and $1/1$) are clearly seen. (b) shows a blow up of V_y from (a), for $f_y = 0.6f_0$ to $2.1f_0$, where additional plateaus at $1/5$, $1/4$, $2/5$, $3/7$, and $3/5$ can be seen more clearly. The overall structure in V_y is that of a Devil's staircase [1-3].

FIG. 2. The vortex trajectories for a subset of the system in Fig. 1 at the plateau regions (a) $f_y/f_x = 0$, (b) $f_y/f_x = 1/2$, and (d) $f_y/f_x = 1/1$, and at the non-plateau region (c) $f_y/f_x = 2\pi/11 = 0.571\dots$. At the plateau regions, the vortices move in 1D channels, periodically along the pinning rows; while at the non-plateau regions the vortices exhibit quasiperiodic trajectories.

FIG. 3. The fraction of (a) six-fold P_6 and (b) four-fold P_4 coordinated vortices versus transverse driving force f_y , for the same system as in Fig. 1. Large drops in P_6 can be seen at f_y^c , as well as at the $1/2$ and $1/1$ locking regions. Smaller dips in P_6 can be seen at the $1/4$, $1/3$, and $2/3$ plateaus regions. At the $1/1$ transition P_4 rises to ≈ 0.9 indicating a transition to a square VL. In (c,d,e) both the vortex positions and Voronoi polygons for a subset of the VL can be seen for: (c) the $1/2$ locking region, where a disordered VL is observed; (d) right before the $1/1$ plateau, with a triangular VL; and (e) at the $1/1$ plateau, with a square VL.

FIG. 4. (a) Phase diagram, for the system in Fig. 1, showing Arnold tongues (shaded); i.e., the widths of the locking regions versus f_p . As f_p decreases, the tongues (locking regions with periodic trajectories) shrink. In (b,c) the width of the first locking region or f_y^c is shown versus pinning lattice constant a (b) and disorder $\delta r/2a$ (c).

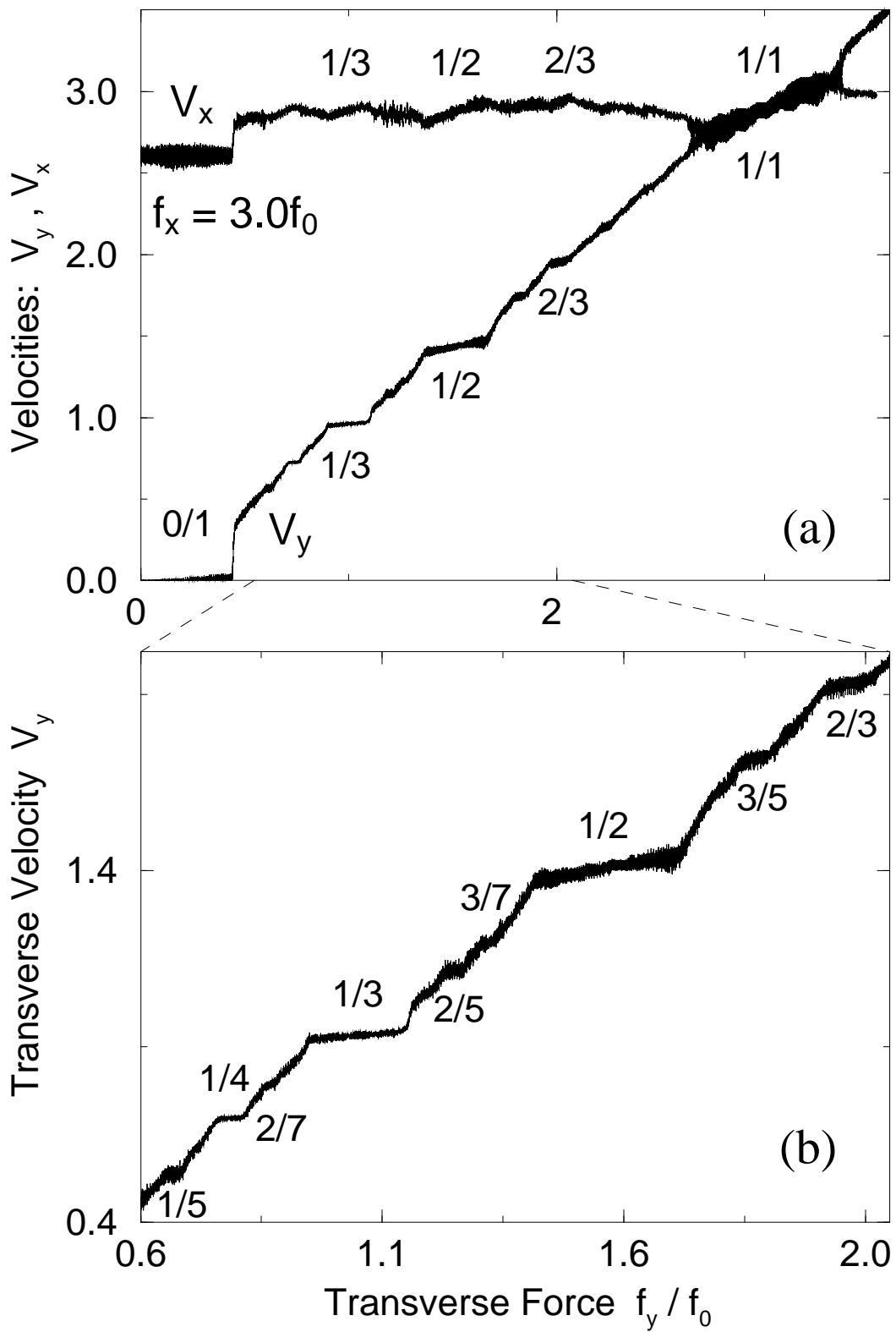


FIG. 1.

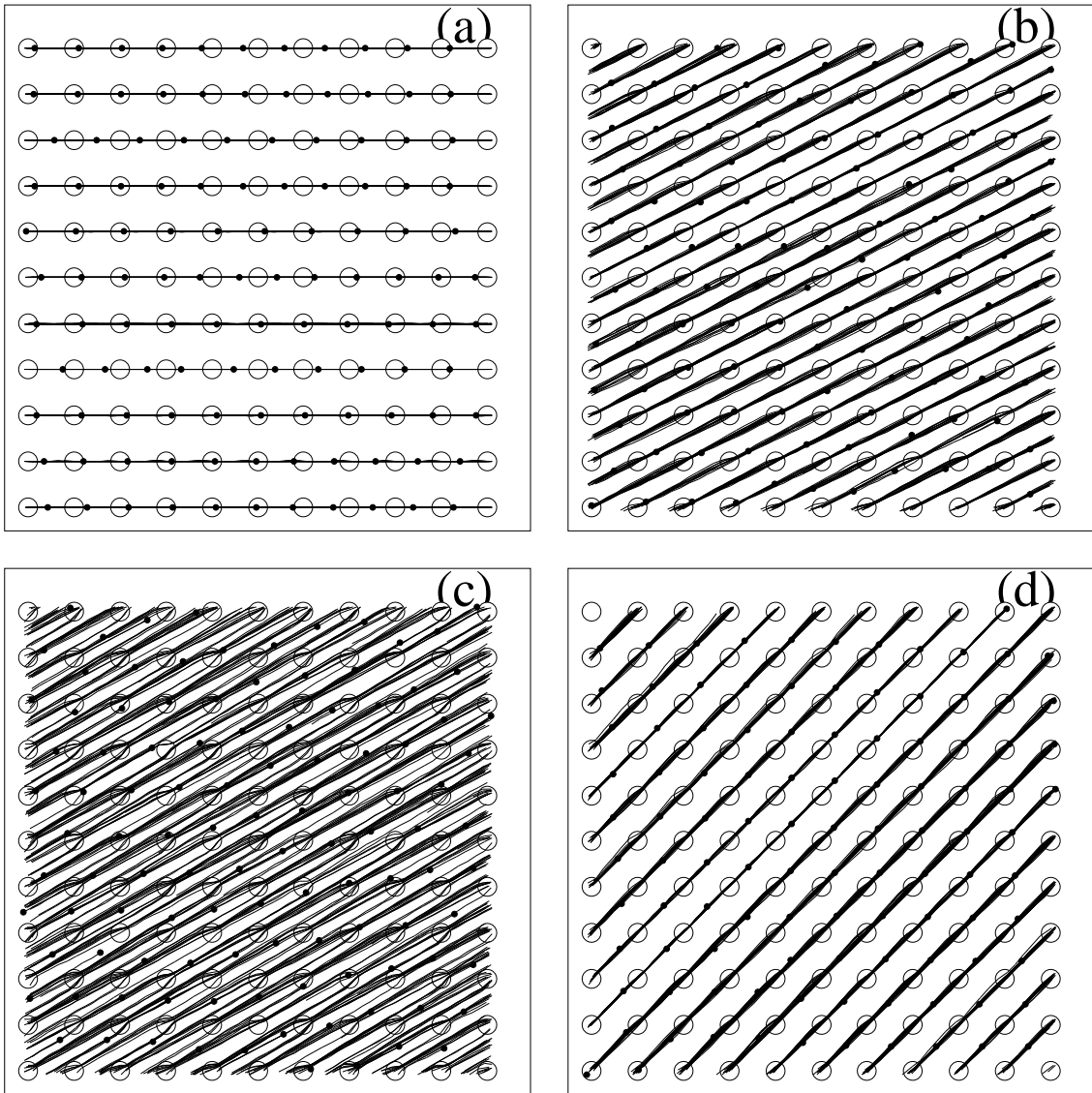


FIG. 2.

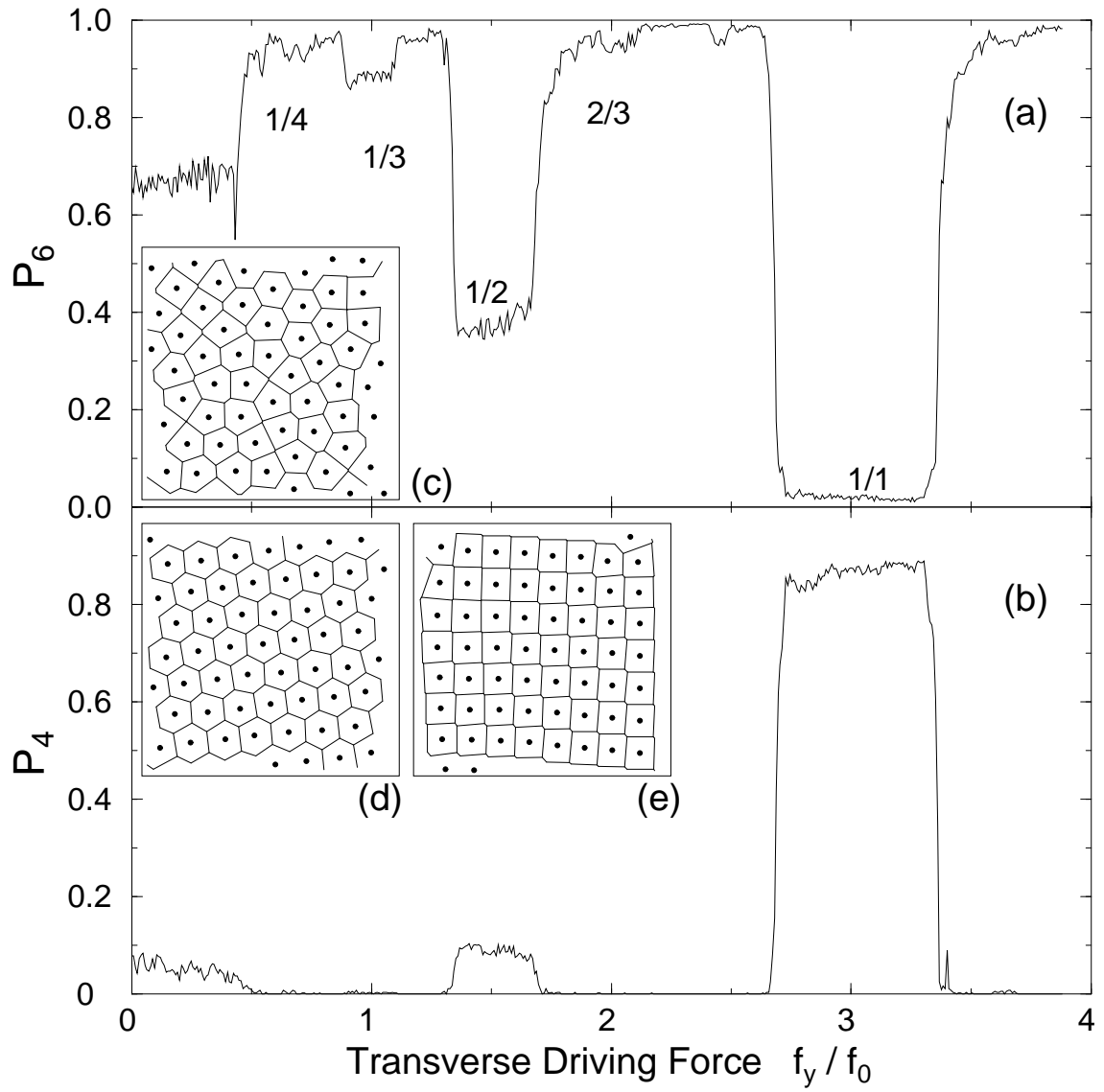


FIG. 3.

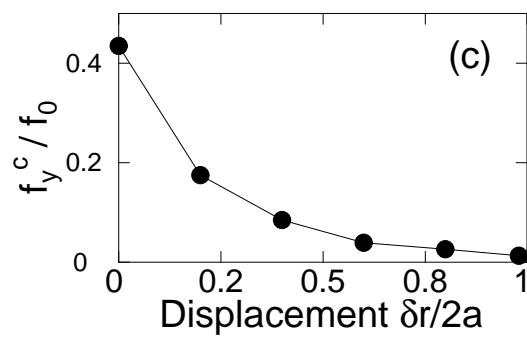
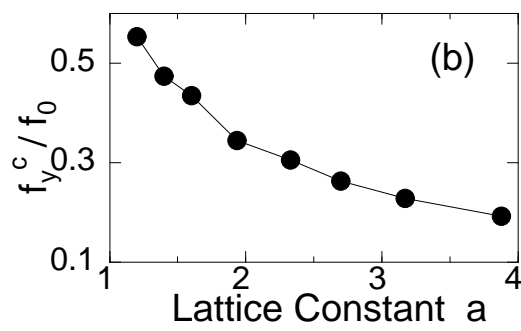
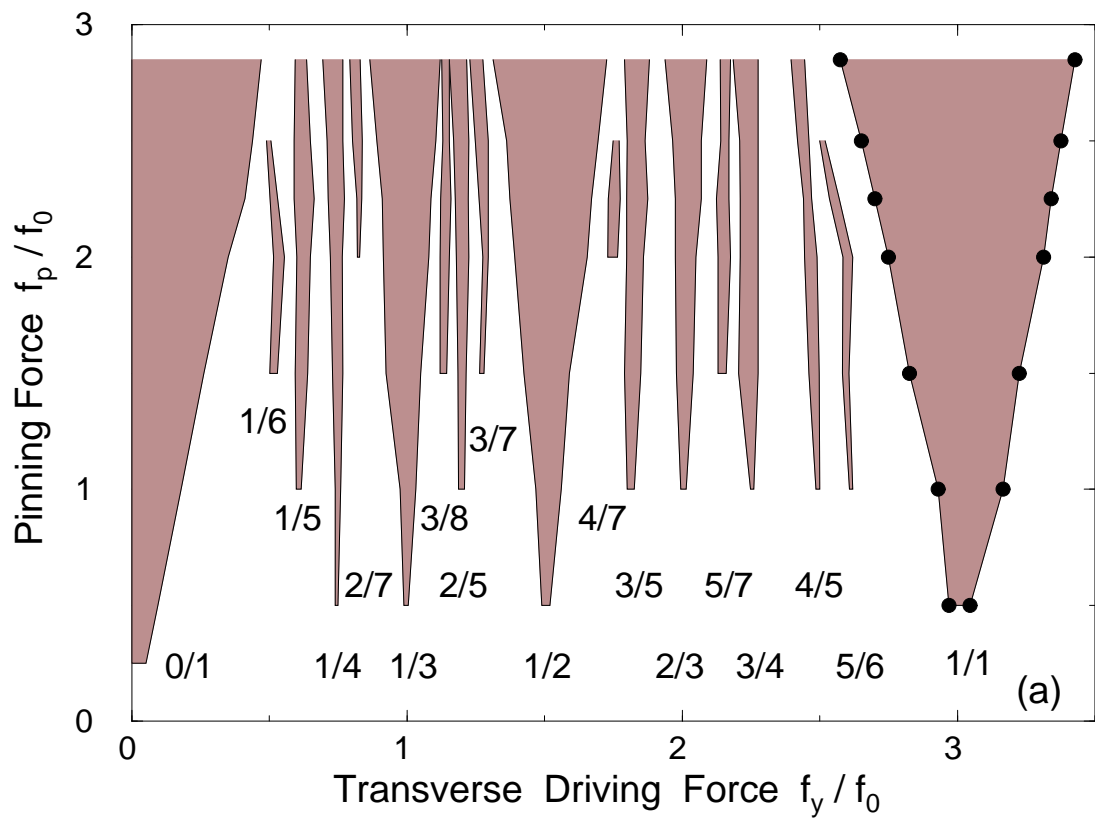


FIG. 4.